10

Application of Porous Media Theories in Marine Biological Modeling

Arzhang Khalili†

Max Planck Institute for Marine Microbiology, Bremen, Germany

Earth and Space Sciences, Jacobs University, Bremen, Germany

Bo Liu, Khodayar Javadi, Mohammad R. Morad, Kolja Kindler

Max Planck Institute for Marine Microbiology, Bremen, Germany

Maciej Matyka

Max Planck Institute for Marine Microbiology, Bremen, Germany

Institute for Theoretical Physics, University of Wrocław, Wrocław, Poland

Roman Stocker

Department of Civil and Environmental Engineering, Massachusetts Institute of Technology, Cambridge, MA

Zbigniew Koza

Institute of Theoretical Physics, University of Wrocław, Wrocław, Poland

CONTENTS

†Corresponding author: Max Planck Institute for Marine Microbiology, Celsiusstr. 1, 28359 Bremen, Germany, Email: akhalili@mpi-bremen.de, Tel.: +49 421 20 28 636, Fax.: +49 421 20 28 690

10.1 Introduction

Theories initially developed to describe transport phenomena through the classical porous medium "soil" and "ground" (Darcy 1856) are encountered literally everywhere in everyday life, in nature, and in technical applications. The reason is that except metals, some plastics and dense rocks, almost all solids and semisolid materials can be considered as "porous" to varying degrees. Hence, there exist many types of different technology that depend on or make use of theories in porous media. The most prominent examples are given in the field of (1) hydrology, which deals with the water movement in earth and soil structures (e.g., dams, wells, filter beds, sewage), (2) petroleum engineering, which deals with exploration and production of oil and gas, and (3) chemical engineering (e.g., heterogeneous catalysis, chromatography, in particular, gel chromatography, separation processes using porous polymers, biological, and inorganic membranes). Also it has been long discovered that granular material sintering (Chen et al. 2005) is a very large tonnage technology, where pore structures are significant, and finds application in manufacturing ceramic products, paper, textile, and so forth.

However, the use of porous media theories in the field of marine microbiology is rather new, and was initiated by the discovery of the role of the seabed in regulation of the chemical composition of water masses in world oceans, and with it the role of oceans in the global cycles (Pamatmat and Banse 1969; Smith Jr. and Teal 1973; Sayles 1979; Emerson et al. 1980; Berelson et al. 1982; Glud et al. 1996, 2007; Ivey et al. 2000; Nikora et al. 2002; Oldham et al. 2004).

It has been found that at the bottom of rivers, lakes, sees, and oceans an enhanced transport of solutes and particulate matter can be encountered in a thin layer, which comprises of a tiny portion of the seawater layer from top and a tiny portion of the porewater layer from below, referred to as the benthic boundary layer (BBL). The BBL has been found to have a direct impact on all physical, chemical, biological, and biogeochemical processes occurring in aquatic systems (Boudreau and Jørgensen 2001).

Most direct denitrification rate measurements for continental shelves have been made on fine-grained, muddy sediments, which cover only 30% of global shelf area. The remaining 70% of continental shelf area is covered by sandy sediments. These sandy sediment environments are generally characterized by low organic matter and high pore water dissolved oxygen concentrations, properties typically considered unfavorable for heterotrophic denitrification

(Emery 1968; Vance-Harris and Ingall 2005). However, it is believed that N_2 production in high-permeability coastal sediments may play an important role in the global nitrogen cycle (Rao et al. 2007). This is another important evidence for the significant role of porous media theories in understanding global cycles.

When seabed sediments are permeable, the advective flux predominates the diffusive one (Huettel and Gust 1992a) drastically. In the context of permeable sediments, a variety of interesting phenomena exists in the field of marine microbiology, which can benefit from the knowledge available in porous media. Examples include, but are not limited to, topography effects in nutrient transport into deeper sediment layers (Huettel and Gust 1992b), enhanced bottom transport by gravity waves (Shum 1992a), reactive solute transport below rippled beds (Shum 1992b), and tide-driven deep pore-water flow in intertidal sands flats (Røy and Lee 2008).

Also the classification of different sediment types providing a habitat for marine species depend on how well the physical properties of the sediment have been described. It has been found that, beside permeability and porosity, the knowledge over tortuosity plays a significant role, for example, in exchange processes in the porewater (Iversen and Jørgensen 1993).

Furthermore, a variety of microorganisms inhabit the seabed, which have the ability of altering or influencing the ongoing interfacial exchange. Prominent examples of this group are burrowing animals, which construct U-, V-, or L-shaped tubes into the seabed, and ventilate the overlying seawater and generate an enhanced mixing. Using peristaltic or oscillatory motions, larvae are able to transfer oxygen into deeper sediment layers, and perform an ecologically significant interfacial nutrient exchange (Riisgård and Larsen 2005). Theoretically it seems obvious that the seawater ventilated by the larvae might also penetrate laterally into the ambient sediment, and generate, in addition to the currently accepted diffusive transport, yet another new mode of transport, namely the advective one. Modeling studies considering flow through a composite region made of saturated sediment and pure-fluid layers can provide useful hints bringing more light into this complex and important phenomena of bioirrigation.

Also in the water column of world oceans, a great deal of situations arise where porous media theories can be applied. An interesting example is that of marine aggregates. It has been found that particle settling has a significant effect on the biogeochemistry and ecology of the oceans due to the fact that particles are the key factor for carbon sequestration, and indirectly responsible for the amount of CO_2 that is released into the atmosphere from the seabed (Chisholm 2000; Azam and Long 2001).

When marine particles coagulate, bigger aggregates are formed that sink from the ocean surface down to the seabed within several hours or days depending on their sinking velocity and the ocean depth. The release of nutrients from sinking aggregates into the ambient seawater or vice versa plays an important role for the marine life. Although some simple models exist in which aggregates were considered as solid bodies (Kiørboe et al. 2001), transmission electron microscopy images (Leppard et al. 2004) clearly reveal that aggregates are rather porous organisms. Hence, implementing porous media theories can enhance the current quantitative estimations of the nutrient exchange mediated by the aggregates from one side, and provide an improved picture of biological consequences. Certainly there exist more biogeochemical problems, which are treated by the means of porous media theories, however, we settle for the examples mentioned to not explode the given framework.

This manuscript is organized as follows. First, a brief description of the mathematical model is brought. In the next sections, some recent examples are given with application in the field of marine microbiology. Finally, some concluding remarks and examples of future applications of porous media in marine microbiology and biogeochemistry have been mentioned.

10.2 Description of the Mathematical Model

For the numerical solution of the porous media equations different techniques such as finite difference method, finite element method, and finite volume method have been suggested. However, lattice Boltzmann model (LBM) has proved to be a promising technique to be applied in porous domains (Guo et al. 2002; Jue 2003; Wu et al. 2005). Compared to other numerical methods, LBM has the advantage of being most suitable for parallel algorithms. Besides, LBM is known to have a simple structure, which makes it most attractive for program coding. Being based on lattices, LBM has the ability of tackling complex meshes, dealing with multiphase, multicomponent fluids or domains (Succi 2001), which frequently occur in the field of marine biogeochemistry. For the sake of completeness, only a brief description of the LBM is brought here. The interested reader may refer to Succi (2001) for further details.

10.2.1 BGK Model

The Boltzmann equation describes a fluid from a microscopic viewpoint as an ensemble of discrete particles following the distribution $f = f(\mathbf{u}, \mathbf{x}, t)$, where f is the probability of finding a particle with velocity (or momentum) in the range $(\mathbf{u},\ \mathbf{u} + d\mathbf{u})$ and position in the range $(\mathbf{x},\ \mathbf{x} + d\mathbf{x})$ at time t. Then the discretized Boltzmann equation in D2Q9 lattice is expressed as follows:

$$f_i(\mathbf{x} + \mathbf{e}_i\delta_t, t + \delta_t) - f_i(\mathbf{x}, t) = -\Omega_i(f(\mathbf{x}, t)) \tag{10.1}$$

where the subscript i is the direction of the velocity. Furthermore, δt is the time increment and Ω_i denotes the collision operator. The discrete velocities

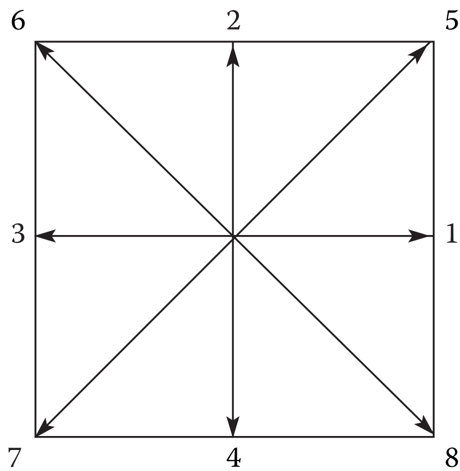

FIGURE 10.1
The lattice direction system for D2Q9 model.

are given by $\mathbf{e}_0 = 0$ and $\mathbf{e}_i = \lambda_i(\cos\theta_i, \sin\theta_i)c$, with $\lambda_i = 1$, $\theta_i = (i-1)\pi/2$ for $i = 1-4$, and $\lambda_i = \sqrt{2}$, $\theta_i = (i-5)\pi/2 + \pi/4$ for $i = 5-8$ (Figure 10.1).

The hydrodynamic variables include mass density (ρ), momentum ($\mathbf{j}$), and flux tensor ($\mathbf{\Pi}$), and are computed by the following:

$$\delta\rho = \sum_i f_i \tag{10.2}$$

$$\mathbf{j} = \rho\mathbf{u} = \sum_i \mathbf{e}_i f_i \tag{10.3}$$

$$\mathbf{\Pi} = \sum_i \mathbf{e}_i\mathbf{e}_i f_i \tag{10.4}$$

Its simplest and by now most popular form is the Bhatnagar–Gross–Krook (BGK) model, which expresses the collision as a relaxation toward a local equilibrium, $\Omega_i = -\frac{1}{\tau}(f_i - f_i^{eq})$, where τ is the nondimensional relaxation time directly related to the kinematic fluid viscosity $\nu = c_s^2\left(\tau - \frac{1}{2}\right)\delta_t$ and $f_i^{(eq)}$ is the equilibrium distribution function (Zou et al. 1995; He and Luo 1997; Dellar 2003):

$$f_i^{(eq)} = \omega_i\rho\left[1 + \frac{\mathbf{e}_i \cdot \mathbf{u}}{c_s^2} + \frac{\mathbf{uu} : (\mathbf{e}_i\mathbf{e}_i - c_s^2\mathbf{I})}{2c_s^4}\right] \tag{10.5}$$

in which ω_i is a weight factor, c_s is the speed of sound (set as $c_s^2 = 1/3$), and $\mathbf{I}$ is the unit tensor. The weights are given by $\omega_0 = 4/9$, $\omega_i = 1/9$ for $i = 1–4$, and $\omega_i = 1/36$ for $i = 5–8$.

The Navier–Stokes equations can be derived from the Chapman–Enskog procedure (Chopard and Droz 1998), which leads to

$$\frac{\partial \rho}{\partial t} + \nabla \cdot (\rho \mathbf{u}) = 0 \tag{10.6}$$

$$\frac{\partial (\rho \mathbf{u})}{\partial t} + \nabla \cdot (\rho \mathbf{u}\mathbf{u}) = -\nabla p + \nu \nabla \cdot [\rho(\nabla \mathbf{u} + \mathbf{u}\nabla)] \tag{10.7}$$

where $p = c_s^2 \rho$ is the pressure, and the effective viscosity is defined as

$$\nu = \tfrac{1}{3}\left(\tau - \tfrac{1}{2}\right)\delta_t \tag{10.8}$$

10.2.2 LBM for Incompressible Flows in Porous Media

Flow in porous media is usually modeled by some semiempirical models because of the complex structure of a porous medium based on the volume averaging at the scale of representative elementary volume (REV). Several widely used models have been introduced in the literature, such as the Darcy, the Brinkman-extended Darcy, and the Forchheimer-extended Darcy models. A recent achievement in modeling flow in porous media is the so-called generalized model, in which all fluid forces and the solid drag force are considered in the momentum equation given by:

$$\nabla \cdot (\mathbf{u}) = 0 \tag{10.9}$$

$$\frac{\partial (\mathbf{u})}{\partial t} + \nabla \cdot \left(\frac{\mathbf{u}\mathbf{u}}{\phi}\right) = -\frac{1}{\rho}\nabla(\phi p) + \nu_e \nabla^2 \mathbf{u} + \mathbf{F} \tag{10.10}$$

In the above equation, ν_e is the effective viscosity and $\mathbf{F}$ represents the total body force given by the following:

$$\mathbf{F} = -\frac{\phi \nu}{K}\mathbf{u} - \frac{\phi F_\phi}{\sqrt{K}}|\mathbf{u}|\mathbf{u} + \phi \mathbf{G} \tag{10.11}$$

in which the three terms on the right side represent Darcy, Forchheimer, and gravity force, respectively. The geometric function F_ϕ and permeability K can be expressed as follows:

$$F_\phi = \frac{1.75}{\sqrt{150\phi^3}} \tag{10.12}$$

$$K = \frac{\phi^3 d_p^2}{\sqrt{150(1-\phi)^2}} \tag{10.13}$$

where d_p is the solid particle diameter.

In the LBM notation, the momentum equation for the fluid flow in a porous medium can be expressed as:

$$f_i(\mathbf{x} + \mathbf{e}_i\delta_t, t + \delta_t) - f_i(\mathbf{x}, t) = -\frac{1}{\tau}\left[f_i(x,t) - f_i^{(eq)}(x,t)\right] + \delta_t F_i \tag{10.14}$$

in which the equilibrium distribution function has been modified as

$$f_i^{(eq)} = \omega_i \rho \left[1 + \frac{\mathbf{e} \cdot \mathbf{u}}{c_s^2} + \frac{\mathbf{uu} : (\mathbf{e}_i \mathbf{e}_i - c_s^2 \mathbf{I})}{2\phi c_s^4} \right] \tag{10.15}$$

and force term as

$$F_i = \omega_i \rho \left(1 - \frac{1}{2\tau} \right) \left[\frac{\mathbf{e}_i \cdot \mathbf{F}}{c_s^2} + \frac{\mathbf{uF} : (\mathbf{e}_i \mathbf{e}_i - c_s^2 \mathbf{I})}{2\phi c_s^2} \right] \tag{10.16}$$

Accordingly, the fluid density and velocity are given by

$$\rho = \sum_i f_i \tag{10.17}$$

$$\mathbf{u} = \frac{\mathbf{v}}{c_0 + \sqrt{c_0^2 + c_1 |\mathbf{v}|}} \tag{10.18}$$

where $\mathbf{v}$ is an auxiliary velocity and is defined as

$$\rho \mathbf{v} = \sum_i \mathbf{e}_i f_i + \frac{\delta_i}{2} \phi \rho \mathbf{G} \tag{10.19}$$

The two parameters c_0 and c_1 are given by

$$c_0 = \frac{1}{2} \left(1 + \phi \frac{\delta_t}{2} \frac{\nu}{K} \right), \quad c_1 = \phi \frac{\delta_t}{2} \frac{F_\phi}{\sqrt{K}} \tag{10.20}$$

By a similar procedure described above, from equation (10.14) one can obtain the extended Darcy equation for a porous medium containing the Brinkman and Forchheimer suggestions as

$$\frac{\partial \rho}{\partial t} + \nabla \cdot (\rho \mathbf{u}) = 0 \tag{10.21}$$

$$\frac{\partial (\rho \mathbf{u})}{\partial t} + \nabla \cdot \left(\frac{\rho \mathbf{uu}}{\phi} \right) = -\nabla (\phi p) + \nabla \cdot [\rho \nu_e (\nabla \mathbf{u} + \mathbf{u} \nabla)] + \rho \mathbf{F} \tag{10.22}$$

where $p = c_s^2 \rho / \phi$ is the pressure, while the effective viscosity is defined as

$$\nu_e = c_s^2 \left(\tau - \frac{1}{2} \right) \delta_t \tag{10.23}$$

10.2.3 LBM for Concentration Release in Porous Media

The LBM for concentration release can be expressed as

$$g_i(\mathbf{x} + \mathbf{e}_i \delta_t, t + \delta_t) - g_i(\mathbf{x}, t) = -\frac{1}{\tau_g} \left[g_i(x, t) - g_i^{(eq)}(x, t) \right] \tag{10.24}$$

where τ_g is the relaxation time and g_i the distribution function for concentration. The equilibrium distribution function was modified as

$$g_i^{(eq)} = \omega_i C \left[\phi + \frac{\mathbf{e} \cdot \mathbf{u}}{c_s^2}\right] \tag{10.25}$$

Accordingly, the concentration and velocity are given by

$$\phi C = \sum_i g_i \tag{10.26}$$

$$\mathbf{u} C = \sum_i g_i c_i \tag{10.27}$$

By a similar procedure described above, from equation (10.14) one can obtain the concentration equation for a porous medium

$$\phi \frac{\partial C}{\partial t} + (\mathbf{u} \cdot \nabla) C = \nabla \cdot [D_m \nabla C] \tag{10.28}$$

with the effective diffusion coefficient

$$D_m = \phi c_s^2 \left(\tau_g - \tfrac{1}{2}\right) \delta_t. \tag{10.29}$$

10.3 Application of Porous Media in Marine Microbiology

As mentioned earlier, in marine microbiology there exists a great deal of situations in which porous media theories apply. From different examples given above, in this section following problems will be discussed: (1) shear-stress control at seabed bottom, (2) tortuosity of marine sediments, (3) oscillatory flows over permeable seabed ripples, (4) nutrient release from sinking marine aggregates, and (5) enhanced nutrient exchange by burrowing macrozoobenthos species.

10.3.1 Shear-Stress Control at Bottom Sediment

In a variety of marine microbiological or environmental issues, generating uniform shear stress planes are desired. An example is given by sampling devices applied in marine sciences—known as microcosms—in which a controlled flow is generated to minimize the erosion threshold by producing a uniform shear stress on the sediment surface.

Recently, shear stress control devices have been considered in technologies for integration of cell separation and protein isolation from mammalian cell cultures. In filtration systems a few circular disks are designed below the rotating cone. This way, due to the fact that shear force, pressure generation, and the specific hydrodynamics of the system are decoupled, shear rates can be easily optimized and precisely controlled to maximize filtration performance while viability of the shear sensitive animal cells is maintained (Vogel et al. 2002).

So far two different categories of devices have been suggested for uniforming the bottom shear stresses. The first one is suggested by Gust (1990), and is composed of a rotating disk in a cylindrical housing. Through the central section of the disk fluid is pumped out and is reentered into the container via the peripheral zone. The disk has optional skirts attached to it (see top image in Figure 10.2).

In the second category, the rotating disk has a conical shape (either flat or curved), and is suggested by Kroner and Vogel (2001) and in modified versions by Sun and Lee (2005) and Ting and Chen (2008). The geometrical configuration of the second category device—termed as shear inducer—has been shown in the middle image in Figure 10.2.

As shown by Khalili et al. (2008), the shear stress uniformity generated by microcosms covers only 72% of the bottom area. A further disadvantage of the microcosm is that it cannot be miniaturized for biological applications such as cell culturing. Also in the case of shear inducers a shear stress uniformity of 84% can be achieved under restricted conditions (very small cone tip-substrate distances, very small Reynolds number). For more details on this issue, the reader is referred to Javadi and Khalili (2009).

As an alternative to the devices in both categories, Khalili and Javadi (2009) have suggested a new device (see the bottom image in Figure 10.2) with which a shear stress uniformity over 94% or larger sections of the bottom area may be generated. As shown in the figure, the system composes of a central rotating disk, surrounded by a number of rings that rotate with lower angular velocities. For the sake of comparison, the shear stress uniformity achieved by all three devices are shown in Figure 10.3. Note that the calculations made for the multiring device contain a central disk and three rotating rings.

As clearly demonstrated, the multiring device performs best. The real advantage of the multiring device is that it can be applied to any flow and size constraints, and can be applied for all kinds of applications both in large and small scale.

Another issue associated with chamber flows and those in cone viscosimeters is the problem of artificial pressure near the interface, which affects directly the sediment-water fluxes. This issue has to be given special attention when the substrate is a porous sediment.

For the sake of completeness, the pressure field has been calculated and plotted in Figure 10.4. The analysis demonstrates an almost contact pressure for the entire radius. The pressure profile generated by the microcosm has two distinct gradients, leading to larger differential pressure. Hence, as far

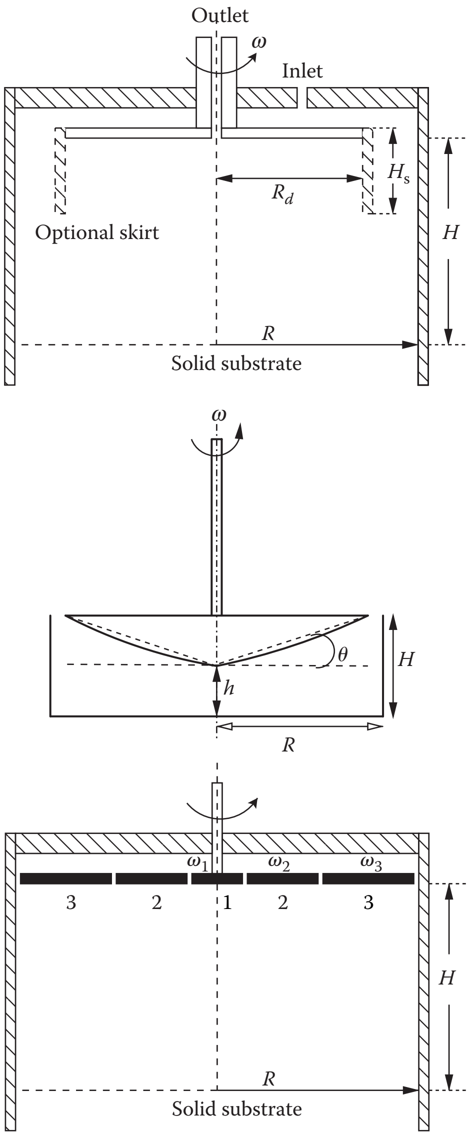

FIGURE 10.2
Geometries of shear stress uniformity devices. Top: microcosm with suction-injection after Gust (1990); middle: rotating cone with flat inclined sides (dashed: after Sun and Lee [2005]) and curved inclined cones (solid lines: after Ting and Chen [2008]) and bottom: multiring device of Khalili and Javadi (2009). Note that here only two rotating rings have been shown. Practically, four or more rings can be implemented to enhance the shear stress uniformity.

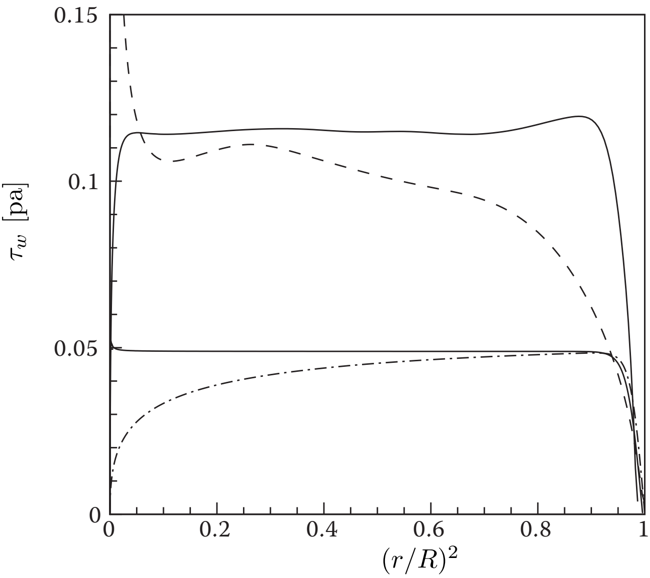

FIGURE 10.3
Shear stress uniformity obtained for three different devices. Dotted line: microcosm of Gust (1990) (Reynolds number is 68672); dashed line: shear inducer device with flat conical sides (Sun and Lee 2005) (cone-substrate distance $h = 100\,\mu$m, cone angle $\alpha = 1°$, angular velocity $\omega = 10$ rpm; solid line: multiring device of (Khalili and Javadi 2009) compared with the microcosm; bold solid line: multiring device miniaturized version.

as the differential pressure is concerned, the multiring device has a better performance.

10.3.2 Tortuosity of Marine Sediments

Permeability and porosity are two important physical properties of any seabed sediment or, in general, any porous media. Beside these two properties, there exists a third quantity known as tortuosity, which significantly influences the ongoing exchange processes in the field of marine geochemistry and geophysics. From hydrodynamic point of view, the tortuosity can be defined as follows: If a fluid particle located in the upstream can migrate on a purely horizontal path to a point downstream within a flow domain, then the tortuosity of the path would be $T = l/L = 1$ with l and L being the path-line length and the geometry length in the flow direction. Hence, the more tortuous the path-line of the fluid particle within a porous medium (because of the existence of solid obstacles) becomes, the larger is T (see Figure 10.5).

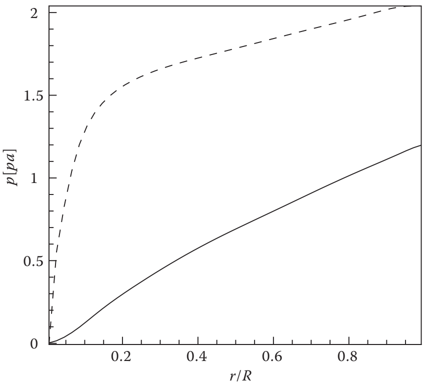

FIGURE 10.4
Distribution of pressure as a function of radius (Reynolds number = 70,000). Dashed line: microcosm of Gust (1990), solid line: multiring device of Khalili and Javadi (2009). The latter device produces an almost constant gradient and lower pressures compared to that of Gust.

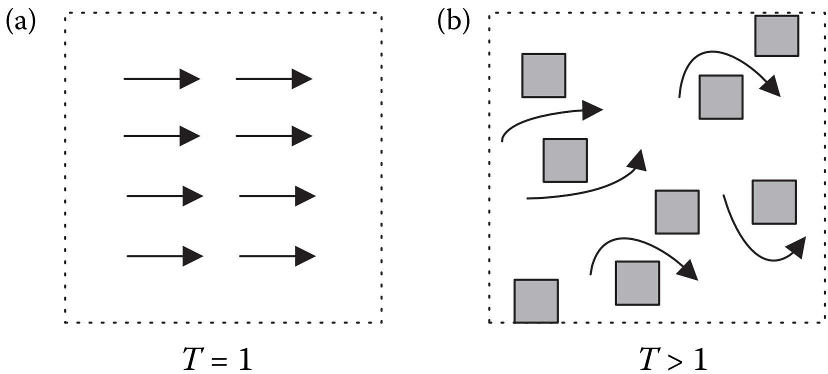

FIGURE 10.5
Comparison of free flow (a) to tortuous flow through a porous structure.

Unfortunately a direct measurement of tortuosity is not possible. This fact has led to diffusive (Nakashima and Yamaguchi 2004), electrical (Lorenz 1961), and acoustic (Johnson et al. 1982) tortuosity definitions. There were also further theoretical attempts by Koponen et al. (1996) to define tortuosity. However, all these tortuosities, in general, differ from each other. Except for some very simple models (Clennell 1997; Knackstedt 1994; Zhang and Knackstedt 1995), there is no clear consensus on its definition. In the literature, so far four different models for tortuosity have been provided given by

$$T(\phi) = \phi^{-p} \tag{10.31}$$

$$T(\phi) = 1 - p \ln \phi \tag{10.32}$$

$$T(\phi) = 1 + p(1 - \phi) \tag{10.33}$$

$$T(\phi) = [1 + p(1 - \phi)]^2 \tag{10.34}$$

with p as a constant factor and ϕ as porosity. The first, second, and third model are theoretical models whereas the fourth one is an empirical model. In sequence, the above equations go back to studies of Archie (1942); Weissberg (1963); Iversen and Jørgensen (1993); and Boudreau and Meysman (2006), respectively.

In a recent study, Matyka et al. (2008) developed an LBM (see Section 10.2) and studied the tortuosity problem from a mathematical perspective. For that purpose, they considered a rectangular flow domain with randomly distributed solid squares as solid obstacles with fixed locations (see Figure 10.6a). By calculating the velocity field and the streamlines (Figure 10.6b) the tortuosity could be calculated, and compared with the models discussed earlier. The comparison shows that the hydrodynamic-based tortuosity calculation of Matyka et al. (2008) matches well with the Weissberg relation (see Figure 10.6c).

For the mathematical modeling presented above, one may ask a question: what is the minimum size of the model system that is able to predict the behavior of the particles in the real world? The underlying basic assumption is that the porous material has to be homogeneous. Large model systems demand high-computational power. This is the main reason why in simulations, system sizes are kept as small as possible. To check this, computational analysis of the path of two particles traveling through a porous medium was performed. Two different alignments with the gravitational field was depicted (see Figure 10.7).

The model system should be homogeneous and should have similar properties in all directions (isotropy). Anisotropy is used to describe the variations of properties depending on the directions. As shown here the model system is too small. Therefore, the traveling particles do not follow direction determined by gravity vector. It was shown by Koza et al. (2009) that the model system has to be at least 100 times larger than the characteristic grain size.

10.3.3 Oscillating Flows over a Permeable Rippled Seabed

The sediment–water interface constitutes a dynamic and significant biologically active region in marine sediments. Within this region, sediments and porewater contact with the overlying water, and exchange between these reservoirs regulates oxygen or nutrient distributions. The importance of the solute transport across this zone has been long recognized as a key factor for accurate determination of sediment oxygen demand in marine environments (Berner 1976).

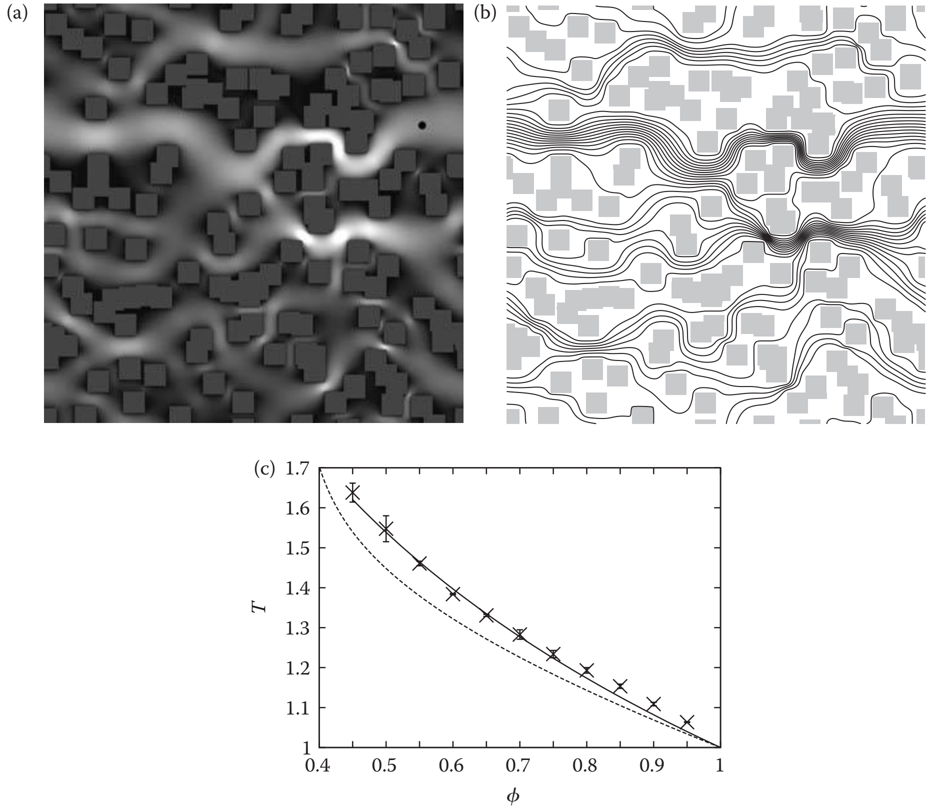

FIGURE 10.6
Calculation of tortuosity in sediments based on path-lines. (a) Velocity magnitudes squared ($u^2 = u_x^2 + v_y^2$). Light gray boxes show randomly placed fixed solid matrices (porosity is 0.7). (b) Streamlines calculated from the velocity field when the flow is induced by the action of gravity. (c) Comparison of tortuosity values calculated from our model (cross symbols with error bars), calculated after Weissberg relation (solid line) and after Koponen et al.

Coastal sediments are often sandy with uneven surfaces, above which the flows is induced into oscillatory motion under surface gravity waves. Gundersen and Jørgensen (1990) measured the vertical distribution of oxygen at the sediment–water interface. They found that the time-averaged concentration was indeed nearly constant except in a thin layer immediately above the sediment surface, where the mean concentration decreased linearly with decreasing elevation. Within this diffusive boundary layer (DBL), which was about 0.6 mm thick, molecular diffusion model was used to estimate the vertical flux of solutes. However, comparisons with actual flux measurements suggested that such an "empirical diffusion coefficient" would have to be a

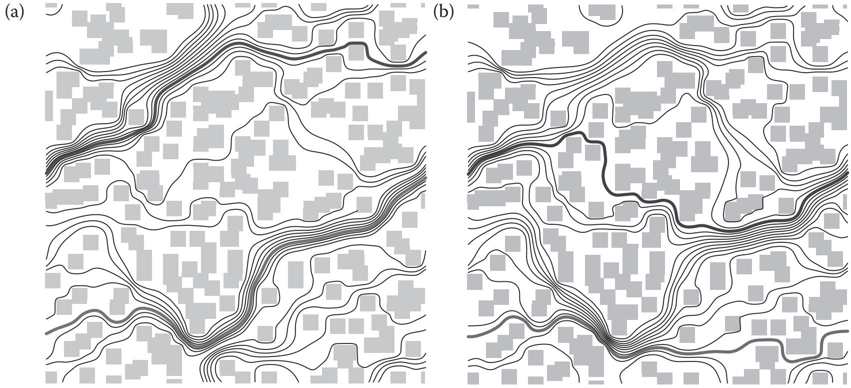

FIGURE 10.7
Computational analysis of the path of two particles traveling through a porous medium. Gravity vector parallel to the x axis (a) and rotated by 20°(b).

few times higher than that of molecular diffusivity. The oxygen concentration in the middle of this DBL oscillated in time with a magnitude of more than 10% of its mean value and at the frequency of the prevalent surface gravity wave. Gundersen and Jørgensen (1990) attributed the oscillations to the "numerous eddies which approach the sediment surface from the bulk of the following sea water and hit the viscous and diffusive sublayers," but details of the physical mechanism involved have yet not been explored.

However, mathematical models for quantifying fluxes across permeable seabeds in the presence of oscillatory flows are, in comparison, not numerous, and limited to the studies of Shum (1992a,b; 1995) and Hara et al. (1992). Although these models provide a good insight into solute distribution below the sediment–water interface, all of them are based on assuming linearized potential flows, and hence, of limited applications. To gain a better understanding of the solute transport in a wave-induced oscillating ambient flow, the LBM model was used to account for both advective and diffusive transport, allowing a clear identification and comparison of fluxes arising from diffusive as well as advective transport (Liu and Khalili 2010a).

In the study, an oscillatory flow has been generated on the surface of the water layer to follow $U = U_0 \sin(\omega t)$ (Figure 10.8) with ω and t being the oscillation frequency and time. The interfacial solute exchange depends on a number of different parameters. The first important parameter is the steepness factor, $s = 2a/L$, which characterizes the sinusoidal ripple. Next, the flow intensity is decided by Reynolds number, $Re = U_0 L/\nu$. Furthermore, the Strouhal number, $St = \pi L/U_0 T)$, describes the oscillating intensity while the Schmidt number, $Sc = \nu/D$, describes the momentum and mass diffusion intensity. In the above relations, $2a, L, U_0, \nu, T$, and D are, respectively, the wave amplitude, the wave length, constant velocity, fluid viscosity, the

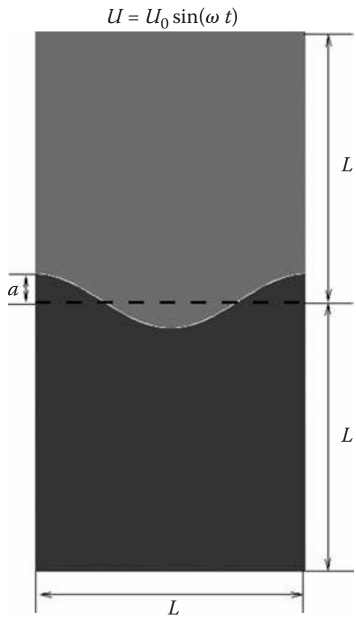

FIGURE 10.8
Illustration of the geometry and flow condition.

oscillation period, and the diffusion coefficient. Finally, the properties of the sediment, the porosity (ϕ) and permeability (k) are also important parameters for the interfacial solute exchange. As the results show, each of the above parameters (Re, St, Sc, s, ϕ, k) are important factors (Liu and Khalili 2010a), however, for the sake of brevity only two cases are shown. These are streamlines at one-quarter and three-quarter period of time, shown in Figure 10.9.

Here we only gave two examples. In Figures 10.10 and 10.11, it has been demonstrated that an increase in the steepness of the ripple and Reynolds number enhanced the advective transport of the solute at the water-sediment interface.

10.3.4 Nutrient Release from Sinking Marine Aggregates

Marine aggregates appear in different forms such as discarded feeding structures, fecal pellets, dead organisms, and other organic debris that sink from the ocean surface down the water depth to the seabed. Depending on their density and diameter, aggregates reach terminal velocities ranging from 15 to 30 m/d, and release/adsorb nutrient into/from the ambient seawater. A typical marine aggregate from the Atlantic with a diameter of 4 mm is shown in

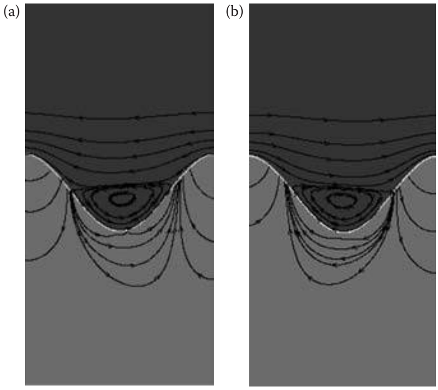

FIGURE 10.9
Streamlines at $t = \mathrm{T}/4$ (a) and $t = 3\mathrm{T}/4$ (b).

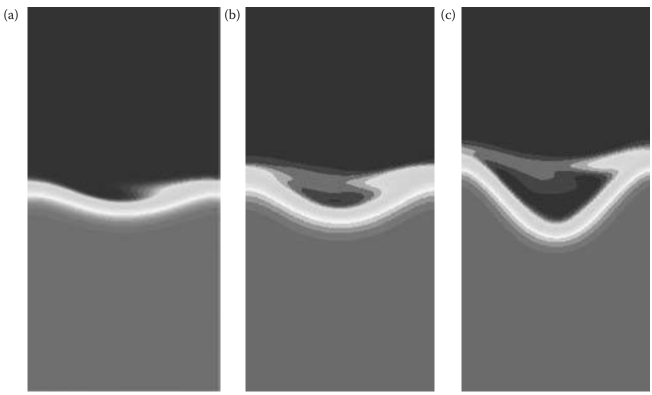

FIGURE 10.10
Solute release in different ripple steepness $s = 0.1$ (a), $s = 0.2$ (b), and $s = 0.4$ (c).

Figure 10.12. This specimen, in common with most from the Atlantic, comprises dead and decaying phytoplankton, zooplankton fecal matter, and their exoskeletons. They sink at rates from a few tens of meters per day to several hundred meters per day in contrast to phytoplankton cells that individually sink at no more than 1 m/d and typically 0.1 m/d.

Owing to this rapid sinking, aggregates are known as a vehicle for vertical flux of organic matter but also hotspots of microbial respiration responsible for a rapid and efficient turnover of particulate organic carbon in the sea (Logan and Wilkinson 1990).

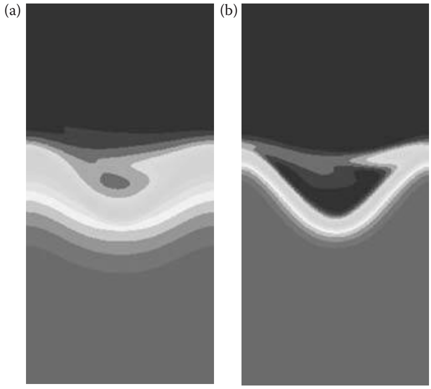

FIGURE 10.11
Solute release at different Reynolds number $Re = 125$ (a) and $Re = 1250$ (b).

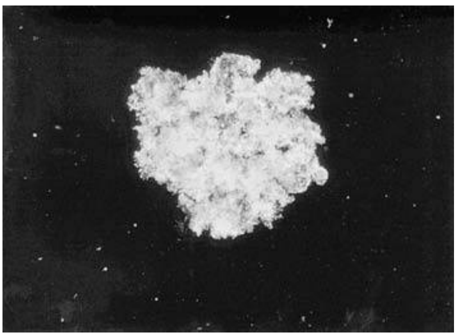

FIGURE 10.12
A marine snow particle of diameter 4 mm. (Courtesy of R. Lampitt.)

This is the reason for the increased interest of the marine scientists in understanding the sinking and exchange mechanisms generated by the aggregates. Owing to the fact that *in-situ* and laboratory-experiments on living aggregates are not an easy task, attempts have been made to simulate their sinking procedure with mathematical techniques.

Until recently, the only model available in the literature was that of Kiørboe et al. (2001), in which aggregates were considered as a solid sphere. However, as mentioned earlier, transmission electron microscopy images have shown that aggregates have a porous structure (Leppard et al. 2004). Hence, there can be two flow scenarios (Figure 10.13). In the solid case, flow can only bypass the aggregates, whereas, in the porous case, a partial throughflow also exists.

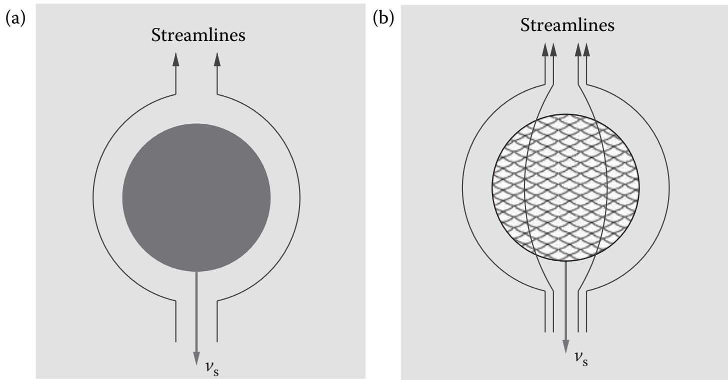

FIGURE 10.13
Schematics of the flow around a solid sphere (a) versus a porous sphere (b). In the latter case a partial throughflow also exits.

More recently, Bhattacharyya et al. (2006) have considered a circular cylindrical porous structure, and showed that porosity and permeability of the aggregate drastically alter the patterns of streamlines, vorticity, and nutrient transfer.

Because the aggregates have, in general, a complex shape, an efficient LBM code has been developed (Liu and Khalili 2008, 2009), which has made possible to treat not only spherical, but also arbitrarily-shaped porous domains (Liu and Khalili 2010b). A comparison between the nutrient release from a solid aggregate versus that of a porous aggregate solved by the model of Liu and Khalili (2010b) can be seen in Figure 10.14. Furthermore, while current calculations have assumed constant porosity, the LBM code can easily account for spatially heterogeneous porosity.

For comparison, a complex geometry is given in Figure 10.15b which consists of four different porous subdomains, a square, a rectangle, an oval, and a circle, which all lie within the same viscous ambient fluid.

As shown in the figure, the flow past the aggregate partially passes through the porous bodies and partially bypasses them. In the example shown, all subdomains have the same fixed porosity of $\phi = 0.993$.

The literature discussed so far invariably assumed a homogeneous fluid density. However, in lakes, oceans, and estuaries, vertical density gradients within the water column are ubiquitous. In freshwater systems, density gradients are caused by a decrease of temperature with depth, while in the ocean it is often salinity that increases with depth. The strength of the stratification is quantified by the Brunt-Väisälä frequency, $N = \sqrt{-(g/\rho_0)(\partial\rho/\partial z)}$, which measures the natural frequency of a fluid parcel in a stable density gradient,

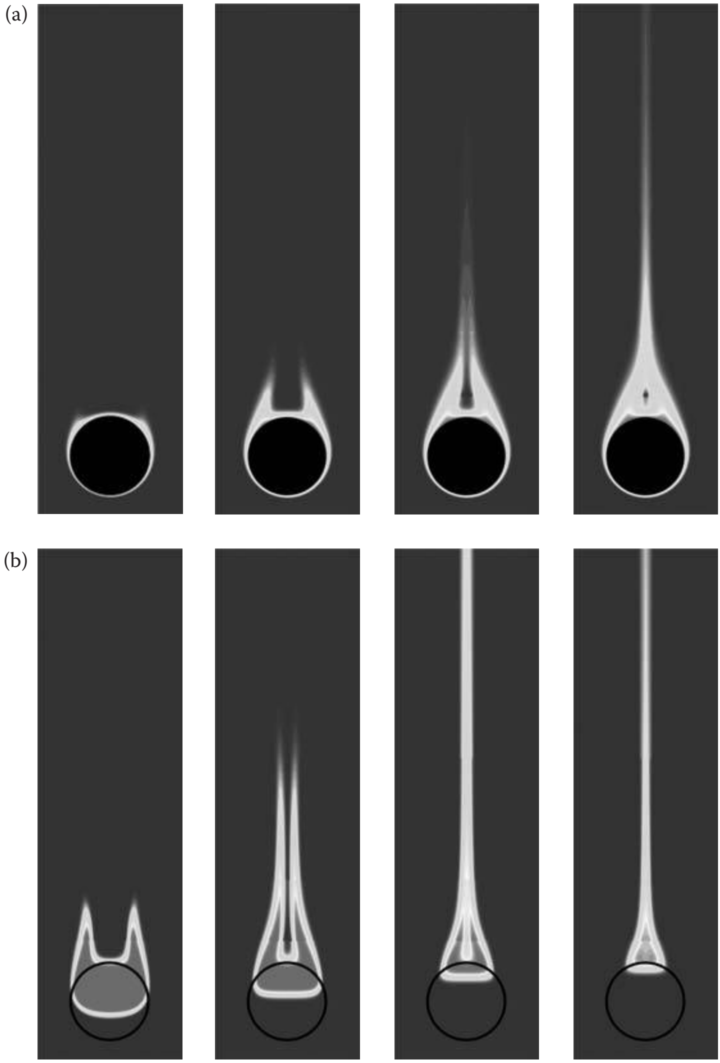

FIGURE 10.14
Release of nutrient from a solid aggregate (a) versus the same from a porous one (b) with a porosity of 0.993 and $Re = 10$. In (a) image, initially a maximum concentration is given at the aggregates surface, which is redistributed with time. In (b), however, the initial maximum concentration covers the entire aggregates interior (the entire sphere is fully red at time $t = 0$, having a maximum concentration). From left to the right, the nondimensional times plotted are 400, 1,000, 2,000, and 3,000, respectively. As can be seen from the figure, the mechanism of concentration release is entirely different in both cases (Liu and Khalili 2008, 2010b).

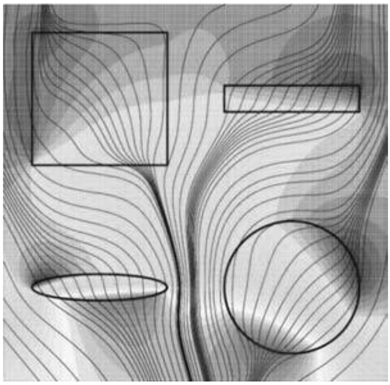

FIGURE 10.15
Streamlines (solid black lines) through and around a complex rectangular cell containing four different porous geometries (square, rectangle, ellipse, and circle). The gray contours represent the pressure distribution (high pressure below the circle and ellipse, low pressure at upper sides of the all geometries).

where g and ρ_0 denote acceleration due to gravity and a reference density, respectively. Naturally occurring stratifications range from $N \approx 0.01\,\mathrm{s}^{-1}$ in the ocean to $N \approx 0.2\,\mathrm{s}^{-1}$ in estuaries or fjords (Farmer and Ami 1999).

Stratification can have a significant impact on an important aspect of the marine carbon cycle, since the sedimentation of particulate organic matter is the main vector of carbon export from surface waters to the deep sea. Particles also affect marine ecology by providing an important resource for planktonic microorganisms. Marine particles of size $a \geq 0.5\,\mathrm{mm}$ are commonly referred to as marine snow. Marine snow typically consist of vestiges of phyto- and zooplankton, together with gel-like transparent exopolymer particles (TEP). Marine snow has high porosity, $\epsilon \geq 0.99$, and small excess density with respect to the ambient seawater, $\Delta\rho_p = \rho_p - \rho = O(10\,\mathrm{kg/m3})$ (Turner 2002). Because of the latter, the sinking of marine snow is characterized by low Reynolds numbers, $Re = aU/\nu = O(0.1-1)$, where U is the settling velocity and ν is the kinematic viscosity.

Marine snow is known to accumulate at pycnoclines in the ocean, forming thin layers that can persist for days and have highly elevated particle concentrations (McIntyre et al. 1995; Alldredge et al. 2002; McManus et al. 2003). It has been speculated that the retention of particles at pycnoclines is caused by the slow, diffusion-driven exchange between interstitial and ambient fluid at the pycnocline (Alldredge and Crocker 1995; Alldredge 1999). Diatom aggregates are nearly impermeable to flow (Ploug et al. 2002), hence the hydrodynamic properties of the aggregates are defined primarily by TEP. By reference to comparable gels, the permeability of TEP is estimated as $k \leq O(10^{-17}\,\mathrm{m}^{-2})$ (Jackson and James 1986). The diffusivity D of small molecules like sodium chloride is very nearly the same in TEP and in seawater (Ploug and Passow 2007).

Previous investigations of solid spheres settling through step-like stratifications at comparable Reynolds numbers, $Re = O(1)$, reported a reduction in settling speed at the pycnocline associated with an increase in drag. This excess drag resulted from the buoyancy of a wake of lighter fluid attached to and dragged downward by the particle (Srdic-Mitrovic et al. 1999). The magnitude of this "tailing" effect is governed by the relative importance of inertial and buoyancy forces, measured by the Froude number $Fr = U/(aN)$. A related effect has been observed for solid particles settling in linear stratifications, where a shell of lighter fluid is entrained by the particle, exerting a buoyancy force on the particle that retards its descent (Yick et al. 2007).

To study the effect of porosity on the settling process at a pycnocline, Kindler et al. (2010) recently conducted experiments with hydrogel spheres settling through a thin density interface with $N = 7.2\,\mathrm{s}^{-1}$, using salt as the stratifying agent (Figure 10.16). The Reynolds number Re_0, based on the terminal velocity in the upper (lighter) phase U_0, was $O(0.1-1)$. The porosity of the spheres was $\phi = 0.955$ and the permeability $k = 10^{-15}\,\mathrm{m}^{-2}$, in general agreement with those of marine snow. The settling of porous, impermeable spheres through a pycnocline is based on two processes: the entrainment of lighter fluid from above, and the relaxation of the interstitial fluid (Figure 10.16). Depending on the initial particle excess density with respect to the lower (denser) layer, $\Delta\rho_p = \rho_1 - \rho_{p_0}$, two limiting scenarios were identified. First,

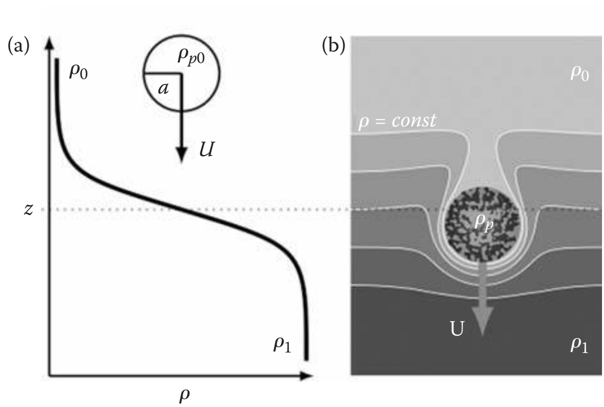

FIGURE 10.16
(a) Schematics of the density stratification. (b) Schematic illustration of the behavior of porous particles settling through a density interface, depending on the initial particle excess density ρ_{p_0} with respect to the lower phase density ρ_1. (From Kindler et al. (2010)).

when $\Delta\rho_p \geq 0$ the sphere decelerates as it enters the heavier layer, due to the decreased specific gravity. The sphere settles in response to the diffusional exchange of fluid from the pore space. In this case, the retention time at the pycnocline scales with the diffusional relaxation time, a^2/D. Second, if $\Delta\rho_p < 0$, particles can sink into the lower layer even in the absence of diffusional exchange of interstitial fluid. For large negative $\Delta\rho_p$, also implying large Re_0, the buoyancy of the interstitial fluid becomes negligible with respect to the effect of entrainment and the particle motion resembles that of a solid sphere in the lower layer.

In conclusion, Kindler et al. (2010) identified and verified a mechanism that can account for porous particle accumulation. However, the coupling of entrainment and diffusive effects for intermediate excess densities has to be clarified to consider more widely occurring, weaker stratifications. A better understanding of marine particle transport and retention within the water column will provide the basis for carbon transport modeling at the basin scale.

10.3.5 Enhanced Nutrient Exchange by Burrowing Macrozoobenthos Species

Chironomid larvae, known also as bloodworms, live on the river bed or lakes in u-tube-like burrows made from detritus (Figure 10.17a). The pupae of midges drift to the surface, where they rest before the adult fly emerges (Figure 10.17b). What makes these species interesting is that they enhance the exchange of dissolved substances between pore water and the overlying water body by their body motion while being in their burrows, and cause the so-called bioirrigation activity.

Microbial consequences and biogeochemical impacts of bioirrigation in benthic sediments have been long recognized and described in studies such as those related to filter feeding (Walshe 1947; Osovitz and Julian 2002), sediment biogeochemistry (Aller 1994; Stief and de Beer 2002; Lewandowski and Hupfer 2005) metabolic demand for oxygen (Polerecky et al. 2006; Timmermann et al. 2006), and the solute exchange between sediment and water (Meysman et al. 2006, 2007).

However, despite their high abundances ($\leq 4{,}000/\mathrm{m}^2$) and their significant ecological role for processes both within and above the sediment, *Chironomus plumosus* provide challenging unsolved questions. Specifically, it was not clear until recently, how to quantify the flow rate pumped into the burrow. Using particle image velocimetry, Morad et al. (2010) and Roskosch et al. (2010) studied three different experimental setups to mimic the natural flow generated by the larvae. For this purpose, a setup was made allowing larvae to burrow their natural tubes in the sediment. A schematics of the burrow has been shown in Figure 10.18a. On the basis of velocity measurements, the volumetric flow rates could be calculated by integrating the velocities obtained by PIV (Figure 10.18b). Rigorous experiments performed showed

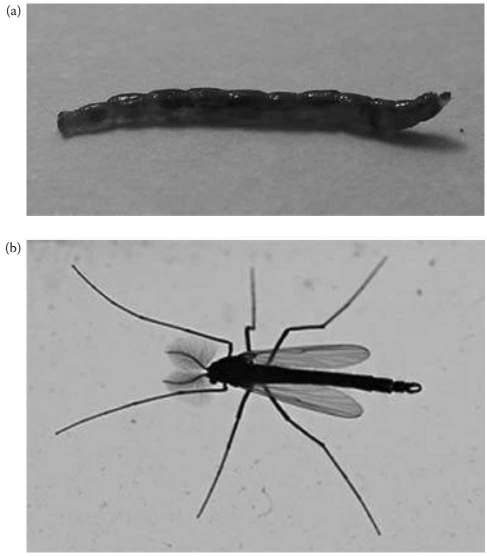

FIGURE 10.17
Chironomus plumosus larva (a) and after adult fly has emerged (b).

that the volumetric flow rates moved by the larvae was between 54.6 and 61.7 mm^3/s.

An early modeling of the effect of tube-dwelling animals was presented by Aller (1980). He defined a microenvironment in marine sediments as a single, tube-dwelling animal together with its surrounding sediment represented by a finite hollow cylinder. Ignoring advection, the transport of solutes within the bioturbated zone was then modeled within a microenvironment given by the diffusion-reaction equation:

$$\frac{\partial C}{\partial t} = D_s \frac{\partial^2 C}{\partial x^2} + \frac{D_s}{r} \frac{\partial}{\partial r}\left(r \frac{\partial C}{\partial r}\right) + R \tag{10.35}$$

where x is depth in sediment relative to the sediment–water interface, r is the radial distance from the center of the tube/burrow, and t is time. Furthermore, the parameters C, D_s, and R are concentration of the dissolved solute, solute diffusion coefficient in bulk sediment, and reaction function, respectively. Equation (10.36) was solved subject to the initial and boundary conditions, such as constant concentration within the burrow by bioirrigation, or continuity of solute flux between the bioturbated and underlying sediment zones. The effect of sediment permeability was taken into account by correcting the diffusion coefficient via tortuosity.

Boudreau and Marinellli (1994) introduced modifications to the cylinder model allowing for periodic bioirrigation because the majority of infaunal

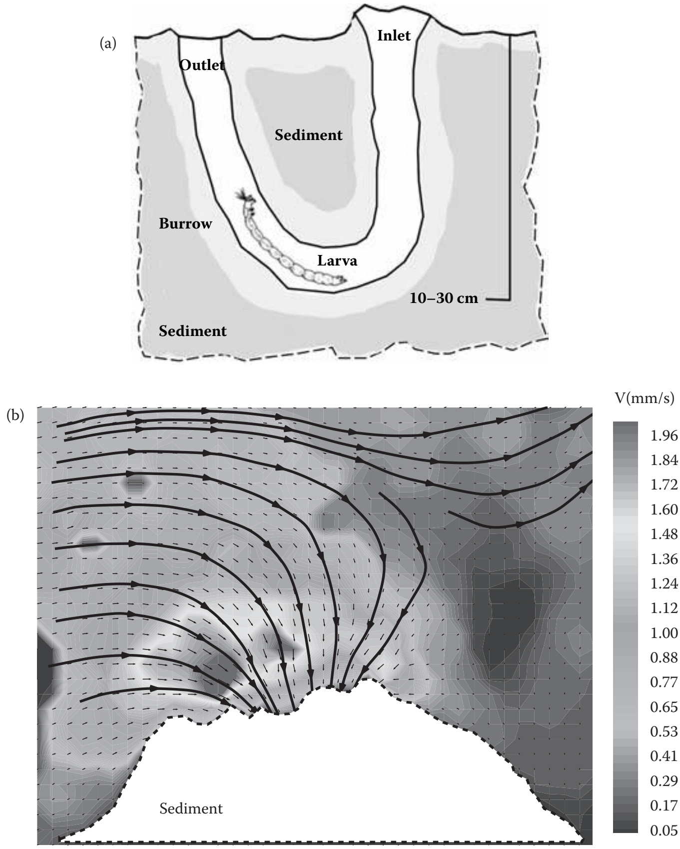

FIGURE 10.18
Schematics of a typical burrow made by *C. plumosus* (a) and the flow visualization near the burrow inlet (b).

burrow-dwelling organisms bioirrigate periodically. This model was further improved by Furukawa et al. (2001) who considered a more realistic depth-dependent distribution of burrows and burrow tilt angles rather than Aller's cylinder model with constant diameter and vertical direction for burrows.

Later, Timmermann et al. (2002) took the effect of advection into account. They injected water from overlying water column into a sediment depth they named Zone 2 (expected to be the feeding depth) to simulate bioturbation by *Arenicola marina*, a bioturbator which irrigates in J-shaped burrows. Zone 1 referred to the sediment above Zone 2, and Zone 3 was below the bioturbated zone where solutes are affected only by diffusion. Timmermann et al. (2002) considered the advection term and solved equation (10.37) considering the effect of sediment porosity in the set of advection–diffusion equations given by

$$\begin{aligned}
&\text{Zone 1:} \quad \frac{\partial \phi C}{\partial t} = \frac{\partial}{\partial x}\left(D\frac{\partial \phi C}{\partial x}\right) + \frac{\partial v\phi C}{\partial x} \\
&\text{Zone 2:} \quad \frac{\partial \phi C}{\partial t} = \frac{\partial}{\partial x}\left(D\frac{\partial \phi C}{\partial x}\right) + \frac{\partial v\phi C}{\partial x} + S(x,t) \\
&\text{Zone 3:} \quad \frac{\partial \phi C}{\partial t} = \frac{\partial}{\partial x}\left(D\frac{\partial \phi C}{\partial x}\right)
\end{aligned} \tag{10.36}$$

where C is the solute concentration in a volume of pore water, ϕ is the porosity, $S(t,x)$ represents the source of solute because of injection of overlying water at feeding depth, $v(t,x)$ is the velocity of the advectively recirculating water and $D(x)$ represent the apparent diffusion coefficient in the sediment. Dividing pumping rate by the area of advection column and sediment porosity, they estimated the advective velocity used in equation (10.36).

A more recent model is presented by Meysman et al. (2006) for the same bioturbator, called the two-dimensional pocket injection model, which was regarded as the advective counterpart of Aller's "diffusive" two-dimensional tube bioirrigation model. They started from Darcy–Brinkman–Forchheimer equation as a general equation to model pore flow and neglected Brinkman-Forchheimer effects because of the low-pore velocity and large-length scales compared to the Brinkman layer involved in the problem, and finally employed the momentum balance reduced to Darcy's law (10.37).

$$v_d = -\frac{k}{\mu}\left(\nabla p - \rho g \nabla x\right) \tag{10.37}$$

In the above equation, k is the permeability, μ is the dynamic viscosity of the pore water, ρ is the pore water density, g is the gravitational acceleration, and x is the vertical coordinate. The Darcy velocity v_d is related to the actual velocity of pore water as $v_d = \phi v$, where ϕ is the porosity. A commercially available code (Comsol Multiphysics) was employed to solve (10.38) and the results were used to solve the reactive transport equations for concentrations.

To date, no exclusive modeling is performed on bioturbation because of U-shape burrows, nor is there any model to contribute the animal's motion characteristics to the flow generated along the burrows and in the sediment.

Beside this issue, there exists still a good number of challenging questions. One of the most prominent one is whether or not the pumping strength of *C. plumosus* is sufficient to mediate an additional advective flow through the burrow walls they construct. Some recent simple models are available for this problem (Shull et al. 1995), however, a real evidence in the form of a two-dimensional flow in a porous-fluid-burrow domain has not yet been provided. Such a model is under development (Morad et al. 2010b) for the geometry shown in Figure 10.19 (a) with a porous sediment having a fixed tube with permeable walls underneath a fluid layer. Using high speed cameras, the equation for the larva's motion has been obtained by digital analysis, and inserted as an input to the model. By solving the momentum equations

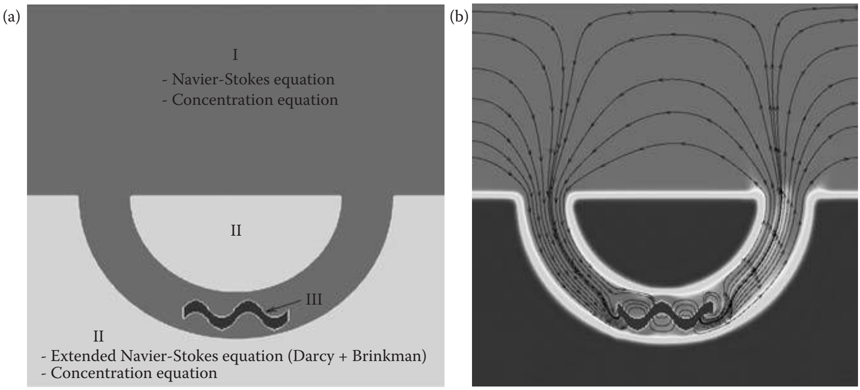

FIGURE 10.19
Geometry of the burrow and the overlying water column with the larva motion simulated (a) and the streamlines and the concentration distribution (gray scale) due to the larva's pumping (b).

as well as the concentration equation, the velocity and concentration field (Figure 10.19) (b) could be obtained precisely. The comparison of the outlet or inlet velocity field obtained in the simulation with the same from the PIV measurements resulted in a good agreement (Morad et al. 2010b).

10.4 Future Prospectives

Porous media applications are ubiquitous not only in technical but also in marine and biological studies, from which some current examples were given in this chapter. However, the real challenge is still to come, namely, in combining visualization and modeling in micro- and nano-scale biology, which, to a larger extent, depends on the progress in multiscale transport processes in complex porous media. Progress in porous media can help characterizing microbial communities to a small scale. Systems approaches require precise analyzes of the spatio-temporal properties of multiple existing microbial environments available in diverse microbiological applications. Exactly, this can be done by the lattice Boltzmann models that are capable of accounting for both the complex structures and the microbial growth and activity on changes to surface wetting induced by surfactants (O'Donnell et al. 2007).

10.5 References

Alldredge, A. L. (1999). The potential role of particulate diatom exudates in forming nuisance mucilaginous scums. *Annali Dell Istituto Superiore di Sanita*, **35**(3):397–400.

Alldredge, A. L. and Crocker, K. M. (1995). Why do sinking mucilage aggregates accumulate in the water column? *Science of the Total Environment*, **165**:15–22.

Alldredge, A. L., Cowles, T. J., McIntyre, S., Rins, J. E. B., Donaghay, P. L., Greenlaw, C. F., Holliday, D. V., Dekshenieks, M. M., Sullivan, J. M., and Zaneveld, J. R. V. (2002). Occurence and mechanisms of formation of a dramatic thin layer of marine snow in shallow Pacific fjord. *Marine Ecology Progress Series*, **233**:1.

Aller, R. C. (1980). Quantifying solute distributions in the bioturbated zone of marine sediments by defining an average microenvironment. *Geochimica Cosmochimica Acta*, **44**:1955–1965.

Aller, R. C. (1994). Bioturbation and remineralization of sedimentary organic matter: effects of redox oscillation. *Chemical Geology*, **114**:331–345.

Archie, G. (1942). The electrical resistivity log as an aid in determining some reservoir characteristics. *Transactions of the American Institute of Mining and Metallurgical Engineers*, **146**:54–62.

Azam, F. and Long, R. A. (2001). Sea snow microcosms. *Nature*, **414**:495–498.

Berelson, W. M., Hammond, D. E., and Fuller, C. (1982). Radon-222 as a tracer for mixing in the water column and benthic exchange in the southern california borderland. *Earth and Planetary Science Letters*, **61**:41–54.

Berner, R. A. (1976). The bentic boundary layer from the viewpoint of a geochemist. In I. N., Mc Cave, ed. *The benthic boundary layer*. Plenum Press, New York.

Bhattacharyya, S., Dhinakaran, S., and Khalili, A. (2006). Fluid motion around and through a porous cylinder. *Chemical Engineering Science*, **61**:4451–4461.

Boudreau, B. P. and Jørgensen, B. B., ed. (2001). *The Benthic Boundary Layer: Transport Processes and Biogeochemistry*. Oxford University Press, Oxford.

Boudreau, B. P. and Marinelli, R. L. (1994). A modelling study of discontinuous biological irrigation. *Journal of Magnetic Resonance*, **52**:947–968.

Boudreau, B. P. and Meysman, F. J. R. (2006). Predicted tortuosity of muds. *Geology*, **34**:693–696.

Chen, D., Mioshi, H., Akai, T., and Yazawa, T. (2005). Colorless transparent fluorescence material: Sintered porous glass containing rare-earth and transition-metal ions. *Applied Physics Letters*, **86**:231908–1–231908–3.

Chisholm, A. W. (2000). Oceanography: stirring times in the southern ocean. *Nature*, **407**:685–687.

Chopard, B. and Droz, M. (1998). *Cellular Automata Modeling of Physical Systems*. Cambridge University Press, Collection Aléa.

Clennell, M. B. (1997). Tortuosity: a guide through the maze. *Geological Society, London, Special Publications*, **122**:299–344.

Darcy, H. P. G. (1856). *Les fontaines publiques de la ville de Dijon*. Victor-Dalmont, Paris.

Dellar, P. J. (2003). Incompressible limits of lattice boltzmann equations using multiple relaxation times. *Journal of Computational Physics*, **190**:351–370.

Emerson, S., Jahnke, R., Bender, M., Froelich, P., Klinkhammer, G., Bowser, C., and Setlock, G. (1980). Early diagenesis in sediments from the eastern equatorial pacific, i. pore water nutrient and carbonate results. *Earth and Planetary Science Letters*, **49**:57–80.

Emery, K. O. (1968). Relict sediments on continental shelves of the world. *American AAPG Bulletin*, **52**:52.

Farmer, D. and Ami, L. (1999). The generation and trapping of solitary waves over topography. *Science*, **283**:188.

Furukawa, Y., Samuel, S. J., and Lavoie, D. L. (2001). Bioirrigation modeling in experimental benthic mesocosms. *Journal of Magnetic Resonance*, **59**:417–452.

Glud, R., Forster, S., and Huettel, M. (1996). Influence of radial pressure gradients on solute exchange in stirred benthic chambers. *Marine Ecology Progress Series*, **141**:303–311.

Glud, R. N., Berg, P., Fossing, H., and Jørgensen, B. B. (2007). Effect of diffusive boundary layer on benthic mineralization and O_2 distribution: a theoretical model analysis. *Journal of Limnology and Oceanography*, **52**: 547–557.

Gundersen, J. K. and Jørgensen, B. B. (1990). Microstructure of diffusive boundary layers and the oxygen uptake of the sea floor. *Nature*, **345**: 604–607.

Guo, Z., Zheng, C., and Shi, B. (2002). Discrete lattice effects on the forcing term in the lattice boltzmann method. *Physics Review E*, **65**:046308.

Gust, G. (1990). Patent US-4,973,165.

Hara, T., Mei, C. C., and Shum, K. T. (1992). Oscillating flows over periodic ripples of finite slope. *Physics of Fluids*, **4**:1373–1384.

He, X. and Luo, L.-S. (1997). Lattice boltzmann model for the incompressible Navier–Stokes equation. *Journal of Statistical Physics*, **88**: 927–944.

Huettel, M. and Gust, G. (1992a). Solute release mechanisms from confined sediment cores in stirred benthic chambers and flume flows. *Marine Ecology Progress Series*, **82**:187–197.

Huettel, M. and Gust, G. (1992b). Impact of bioroughness on interfacial solute exchange in permeable sediments. *Marine Ecology Progress Series*, **89**:253–267.

Iversen, N. and Jørgensen, B. B. (1993). Diffusion coefficients of sulfate and methane in marine sediments: Influence of porosity. *Geochimica Cosmochimica*, **57**:571–578.

Ivey, G. N., Winters, K., and Silva, I. P. D. S. D. (2000). Turbulent mixing in a sloping benthic boundary layer energized by internal waves. *Journal of Fluid Mechanics*, **48**:59–76.

Jackson, G. W. and James, D. F. (1986). The permeability of fibrous media. *Canadian Journal of Chemical Engineering*, **64**:364–374.

Javadi, K. and Khalili, A. (2009). On generating uniform bottom shear stress. Part II: shear stress inducing devices. *Recent Patents in Chemical Engineering*, **2**(3):223–229.

Johnson, D. L., Plona, T. J., Scala, C., Pasierb, F., and Kojima, H. (1982). Tortuosity and acoustic slow waves. *Physics Review Letters*, **49**:1840–1844.

Jue, T.-C. (2003). Numerical analysis of vortex shedding behind a porous square cylinder. *International Journal of Numerical Methods for Heat and Fluid Flow*, **14**:649–663.

Khalili, A. and Javadi, K. (2009). How to produce uniform shear stress? In preparation.

Khalili, A., Javadi, K., Saidi, A., Goharzadeh, A., Huettel, M., and Jørgensen, B. B. (2008). On generating uniform bottom shear stress, Part I: a quantitative study of microcosm chamber. *Recent Patents in Chemical Engineering*, **1**:174–191.

Kindler, K., Khalili, A., and Stocker, R. (2010). Accumulation of porous particles settling through pycnoclines. Submitted.

Kiørboe, T., Ploug, H., and Thygesen, U. H. (2001). Fluid motion and solute distribution around sinking aggregates. I. Small-scale fluxes and heterogeneity of nutrients in the pelagic environment. *Marine Ecology Progress Series*, **211**:1–13.

Knackstedt, M. A. (1994). Direct evaluation of length scales and structural parameters associated with flow in porous media. *Physics Review E*, **50**:2134–2138.

Koponen, A., Kataja, M., and Timonen, J. (1996). Tortuous flow in porous media. *Physics Review E*, **54**:406–410.

Koza, Z., Matyka, M., and Khalili, A. (2009). Finite-size anisotropy in statistically uniform porous media. *Physics Review E*, **79**:066306–1–066306–7.

Kroner, K. and Vogel, J. (2001). US20016193883B1.

Leppard, G. G., Mavrocordatos, D., and Perret, D. (2004). Electron-optical characterization of nano- and micro-particles in raw and treated waters: an overview. *Water Science and Technology*, **50**:1–8.

Lewandowski, J. and Hupfer, M. (2005). Effect of macrozoobenthos on two-dimensional smallscale heterogeneity of pore water phosphorus concentrations in lake sediments: a laboratory study. *Limnology Oceanography*, **50**:1106–1118.

Liu, B. and Khalili, A. (2008). Acceleration of steady-state Lattice Boltzmann simulation for exterior flow. *Physics Review E*, **78**:056701–1–056701–9.

Liu, B. and Khalili, A. (2009). Lattice Boltzmann model for exterior flows with an annealing preconditioning method. *Physics Review E*, **79**:066701–1–066701–7.

Liu, B. and Khalili, A. (2010a). Oscillatory flow over permeable beds, In preparation.

Liu, B. and Khalili, A. (2010b). Concentration release from sinking aggregates of an arbitrary shape, in preparation.

Logan, B. E. and Wilkinson, D. B. (1990). Fractal geometry of marine snow and other biological aggregates. *Limnology Oceanography*, **35**:130–136.

Lorenz, P. B. (1961). Tortuosity in porous meida. *Nature*, **189**:386–387.

Matyka, M., Khalili, A., and Koza, Z. (2008). Tortuosity–porosity relation in porous media flow. *Physics Review E*, **78**:026306–1–026306–8.

McIntyre, S., Alldredge, A. L., and Gotschalk, C. C. (1995). Accumulation of marine snow at density discontinuities in the water column. *Limnology and Oceanography*, **40**(3):449–468.

McManus, M. A., Alldredge, A. L., Barnard, A., Boss, E., Case, J. F., Cowles, T. J., Donaghay, P. L., Eisner, L. B., Gifford, D. J., Greenlaw, C. F., Herren, C. M., Holliday, D. V., Johnson, D., McIntyre, S., McGehee, D. M., Osborne,

T. R., Perry, M. J., Pieper, R. E., Rines, J. E. B., Smith, D. C., Sullivan, J. M., Talbot, M. K., Twardowski, M. S., Weidmann, A., and Zaneveld, J. (2003). Characteristics, distribution and persistence of thin layers over a 48 hour period. *Marine Ecology Progress Series*, **261**:1.

Meysman, F. J. R., Galaktionov, O. S., Cook, P. L. M., Janssen, F., Huettel, M., and Middelburg, J. J. (2007). Quantifying biologically and physically induced flow and tracer dynamics in permeable sediments. *Biogeosciences*, **4**:627–646.

Meysman, F. J. R., Galaktionov, O. S., Gribsholt, B., and Middelbur, J. J. (2006). Bioirrigation in permeable sediments: advective porewater transport induced by burrow ventilation. *Journal of Limnology and Oceanography*, **51**:142–156.

Morad, M. R., Khalili, A., Roskosch, A., and Lewandowski, J. (2010). Quantification of pumping rate by chironomus plumosus larvae in real burrows. *Aquatic Ecology*, **44**(1):143–153.

Morad, M. R., Liu, B., and Khalili, A. (2010). Hydrodynamics generated by the *C. Plumosus* larva: an experimental and mathematical study, in preparation.

Nakashima, Y. and Yamaguchi, T. (2004). DMAP.m: a mathematica program for three-dimensional mapping of tortuosity and porosity of porous media. *Bulletin of the Geological Survey of Japan*, **55**:93–103.

Nikora, V., Goring, D., and Ross, A. (2002). The structure and dynamics of the thin near-bed layer in a complex marine environment: A case study in Beatrix Bay, New Zealand. *Estuarine, Coastal and Shelf Science*, **54**: 915–926.

O'Donnell, A. G., Young, I. M., Rushton, S. P., Shirley, M. D., and Crawford, J. W. (2007). Visualization, modelling and prediction in soil microbiology. *Nature Reviews Microbiology*, **5**:689–699.

Oldham, C. E., Ivey, G. N., and Pullin, C. (2004). Estimation of a characteristic friction velocity in stirred benthic chambers. *Marine Ecology Progress Series*, **279**:291–295.

Osovitz, C. J. and Julian, D. (2002). Burrow irrigation behaviour of *Urechis caupo*, a filter-feeding marine invertebrate, in its natural habitat. *Marine Ecology Progress Series*, **473**:149–155.

Pamatmat, M. M. and Banse, K. (1969). Oxygen consumption by the seabed. ii. in situ measurements to a depth of 180 m. *Journal of Limnology and Oceanography*, **14**:250–259.

Ploug, H. and Passow, U. (2007). Direct measurements of diffusivity within diatom aggregates containing transparent exopolymer particles. *Limnology and Oceanography*, **52**:1–6.

Polerecky, L., Volkenborn, N., and Stief, P. (2006). High temporal resolution oxygen imaging in bio-irrigated sediments. *Environmental Science Technology*, **40**:5763–5769.

Rao, A. M. F., Mccarthy, M. J., Gardner, W. S., and Jahnke, R. A. (2007). Respiration and denitrification in permeable continental shelf deposits on the south atlantic bight: Rates of carbon and nitrogen cycling from sediment column experiments. *Continental Shelf Research*, **27**:1801–1819.

Riisgård, H. U. and Larsen, P. S. (2005). Water pumping and analysis of flow in burrowing zoobenthos—an overview. *Journal of Experimental Biology*, **198**:283–294.

Roskosch, A., Morad, M. R., Khalili, A., and Lewandowski, J. Bioirrigation by Chironomus plumosus: advective flow investigated by particle image velocimetry. Accepted.

Røy, H. and Lee, J. S. (2008). Tide-driven deep pore-water flow in intertidal sands flats. *Limnology Oceanography*, **53**:1521–1530.

Sayles, F. L. (1979). The composition and diagenesis of interstitial solutions. fluxes across the seawater–sediment interface in the atlantic ocean. *Geochimica Cosmochimica Acta*, **43**:527–545.

Shull, D., Benoit, J., Wojcik, C., and Senning, J. (1995). Infaunal burrow ventilation and pore-water transport in muddy sediments. *Estuarine, Coastal, and Shelf Science*, **83**:277–286.

Shum, K. T. (1992a). Wave-induced advective transport below a rippled water-sediment interface. *Journal of Geophysics Research*, **97**(C1):789–808.

Shum, K. T. (1992b). The effects of wave-induced pore water circulation on the transport of reactive solutes below a rippled sediment bed. *Journal of Geophysics Research*, **98**(C6):10289–10301.

Shum, K. T. (1995). A numerical study of the wave-induced solute transport above a rippled bed. *Journal of Fluid Mechanics*, **299**:267–288.

Smith Jr., K. L. and Teal, J. M. (1973). Deep-sea benthic community respiration: an in situ study at 1850 meters. *Science*, **179**:282–283.

Srdic-Mitrovic, A. N., Mohamed, N. A., and Fernando, H. J. S. (1999). Gravitational settling of particles through density interfaces. *Journal of Fluid Mechanics*, **381**:175–198.

Stief, P. and de Beer, D. (2002). Bioturbation effects of chironomus riparius on the benthic n-cycle as measured using microsensors and microbiological assays. *Aquatic Microbial Ecology*, **2**:175–185.

Succi, S. (2001). *The Lattice Boltzmann Equation for Fluid Dynamics and Beyond*. Oxford University Press, Oxford.

Sun, M. and Lee, S. (2005). US20050032200.

Timmermann, K., Banta, G. T., and Glud, R. N. (2006). Linking arenicola marina irrigation behavior to oxygen transport and dynamics in sandy sediments. *Journal of Marine Research*, **64**:915–938.

Timmermann, K., Christensen, J. H., and Banta, G. T. (2002). Modeling of advective solute transport in sandy sediments inhabited by the lugworm arenicola marina. *Journal of Marine Research*, **60**:151–169.

Ting, T. and Chen, Y. (2008). US20080038816A1.

Vance-Harris, C. and Ingall, E. (2005). Denitrification pathways and rates in the sandy sediments of the georgia continental shelf, USA. *Geochemical Transactions*, **6**(1):12–18.

Vogel, H., Anspach, B., Kroner, K., Piret, J., and Haynes, C. (2002). Controlled shear affinity filtration (csaf): A new technology for integration of the cell separation and protein isolation from mammalian cell cultures. *Biotechnology Bioengineering*, **78**:806–814.

Walshe, B. M. (1947). Feeding mechanism of chironomus larvae. *Nature*, **160**:474.

Weissberg, J. (1963). Effective diffusion coefficient in porous media. *Journal of Applied Physics*, **34**:2636–2639.

Wu, H. R., He, Y. L., Tang, G. H., and Tao, W. Q. (2005). Lattice Boltzmann simulation of flow in porous media on non-uniform grids. *Progressive Computational Fluid Dynamics*, **5**(1/2):97–103.

Zhang, X. and Knackstedt, M. A. (1995). Direct simulation of electrical and hydraulic tortuosity in porous solids. *Geophusics Research Letters*, **22**:2333–2338.

Zou, Q., Hou, S., and Doolen, G. D. (1995). Analytical solutions of the lattice boltzmann bgk model. *Journal of Statistical Physics*, **81**(1/2):319–334.